

# High-Efficiency and Low Distortion Photoacoustic Effect in 3D Graphene Sponge

Flavio Giorgianni, Carlo Vicario, Mostafa Shalaby, Lorenzo Donato Tenuzzo, Augusto Marcelli, Tengfei Zhang, Kai Zhao, Yongsheng Chen,\* Christoph Hauri, and Stefano Lupi\*

The conversion of light in sound plays a crucial role in spectroscopy, applied physics, and technology. In this paper, light-sound conversion in 3D graphene sponge through a photo-thermoacoustic mechanism is reported. It is shown that the unique combination of mechanical, optical, and thermodynamic properties of graphene assembled in a 3D sponge structure allows an unprecedented high efficiency conversion independent of light wavelength from infrared to ultraviolet. As a first application of this effect, a photothermal based graphene sponge loudspeaker is demonstrated, providing a full digital operation for frequencies from acoustic to ultrasound. The present results suggest a new pathway for light generation and control of sound and ultrasound signals potentially usable in a variety of new technological applications from high-fidelity loudspeaker and radiation detectors to medical devices.

## 1. Introduction

Sound generation has been explored for millennia for communications, enjoyment, and cultural reasons.<sup>[1]</sup> In the contemporary society, sound generation and recording are even more important and efficient small-scale loudspeakers or contactless communication devices represent a cutting-edge technology for daily life.

For human audibility, an ideal speaker should generate a uniform sound pressure level (SPL) in the frequency range 20 Hz to 20 kHz. Most of loudspeakers commercially available today, are based on a thin membrane connected to a voice coil nested in a permanent magnet. When alternating current passes through the coil, mechanical oscillations of the membrane are produced, leading adiabatic compressions and expansions of the surrounding air, i.e., sound. However, the electromechanical resonances underlying this sound generation mechanism has an inherently narrow frequency response.<sup>[2]</sup> As a matter of fact, it is not possible to cover with a single mechanical loudspeaker the entire spectrum from acoustic region to ultrasound and this represents the major limitation for high-fidelity reproduction of a real sound.

A first nonmechanical sound emission mechanism has been discovered in 1880 by Bell.<sup>[3–6]</sup> Bell found that when a pulsed light beam shines both solids, liquids, and gases, an audible sound is generated. His work generated a flurry of interest until recent years where photoacoustic emission is used as a powerful spectroscopic technique in condensed matter physics.<sup>[7]</sup> Another sound emission mechanism has been investigated by Arnold and Crandall.<sup>[8]</sup> Here, sound is produced through a conversion of heat energy in pressure waves and is called thermoacoustic effect. More specifically, when an alternating current passes through a material a time dependent Joule heat is generated and then converted in sound which may extend beyond the acoustic region.

Although thermoacoustic and photoacoustic devices and their combination were conceived a long time ago, only recently the application of nanofabrication techniques allowed to produce acoustic devices based on ultrathin conductive structures,<sup>[9–12]</sup> which permit to increase their conversion efficiency. However, the discovery of new, highly performant, photo-thermoacoustic materials could overcome the actual technical limits representing a cutting-edge technology for daily life.

Dr. F. Giorgianni, L. D. Tenuzzo, Prof. S. Lupi  
Department of Physics  
University of Rome La Sapienza  
P.le A. Moro 2, 00185 Rome, Italy  
E-mail: stefano.lupi@roma1.infn.it; yschen99@nankai.edu.cn

Dr. F. Giorgianni, Dr. C. Vicario, Dr. M. Shalaby, Dr. C. Hauri  
Paul Scherrer Institute  
SwissFEL  
5232 Villigen-PSI, Switzerland

Dr. A. Marcelli  
INFN-LNF  
via E. Fermi 40, 00044 Frascati, Italy

Dr. A. Marcelli  
RICMASS  
Rome International Center for Materials Science Superstripes  
Via dei Sabelli 119A, 00185 Rome, Italy

Dr. A. Marcelli  
CNR – Istituto Struttura della Materia and Elettra-Sincrotrone Trieste  
Basovizza Area Science Park 34149, Trieste, Italy

Dr. T. Zhang, K. Zhao, Prof. Y. Chen  
State Key Laboratory and Institute of Elemento-Organic Chemistry  
Collaborative Innovation Center of Chemical Science and Engineering  
(Tianjin)

Key Laboratory of Functional Polymer Materials and the  
Centre of Nanoscale Science and Technology  
Institute of Polymer Chemistry  
College of Chemistry  
Nankai University  
Tianjin 300071, China

 The ORCID identification number(s) for the author(s) of this article can be found under <https://doi.org/10.1002/adfm.201702652>.

DOI: 10.1002/adfm.201702652

Graphene is the ideal material for the photo thermoacoustic conversion of light because it shows: (i) A low heat capacity necessary to achieve large thermal gradients; (ii) A high thermal conductivity to deliver rapidly heat to the surrounding gas; (iii) An absorption coefficient, due to Dirac-particle-like electronic states,<sup>[13]</sup> practically independent of radiation wavelength from terahertz (THz) to ultraviolet (UV). Those unprecedented combinations of optical, mechanical, and thermal properties candidate graphene as one of the most promising material to transduce light in acoustic waves.

So far graphene loudspeaker has been implemented using thermoacoustic transduction of an electrical signal into heat and sound. These devices are based on a substrate-deposited single-layer graphene to achieve a good mechanical stability.<sup>[14]</sup> Although, the major part of heat is dissipated in the substrate thus reducing the thermoacoustic conversion efficiency,<sup>[14–16]</sup> those thermoacoustic devices are able to operate in a wide frequency range up to tens of kHz.

Recently, it has been observed that the properties of 2D graphene can be extended on a macroscopic scale arranging individual graphene sheets in 3D monolithic structures.<sup>[17–22]</sup> In particular, graphene 3D sponges (G-sponge), while keeping the peculiar characteristics of single-layer graphene, add further interesting properties like an extremely lightness associated to a robust mechanical strength, and a highly repeatable compression and complete volume recovery in a wide temperature range both in air and in liquid without a substantial structure degradation.<sup>[17,18]</sup>

In this paper, we report on the first light-driven loudspeaker based on photo thermo-acoustic effect in graphene-sponges. We found that a G-sponge sample is a highly efficient magnet-free, metal-free, and contactless loudspeaker driven by light. We fully characterized the photoacoustic response as function of the modulation frequency and of the sponge density, revealing a sound emission linearly dependent on light intensity and independent of light wavelength in a broad spectral range from infrared (IR) to UV. The graphene-sponge light-driven loudspeaker covers an acoustic range from 100 Hz to 20 kHz and, ultimately, it plays music from modulated light with negligible harmonic distortion.

## 2. Results

### 2.1. Acoustic Waves in Graphene Sponge Induced by Modulated Light

The scheme of the photoacoustic setup is reported in **Figure 1a**. Intensity modulated light was generated by light emitting diode (LED) sources powered by a modulated electric signal. The emitted light is focused on the G-sponge to a spot size smaller than the sample in an anechoic chamber (see **Figure 1b**). This chamber was used both to acoustically isolate the experimental apparatus from environmental noise and to reduce internal sound reflection interference.

The emitted sound is finally acquired using a calibrated microphone (Samson-C02) placed behind the G-sponge at a fixed distance of 2.5 cm in the far-field region.

3D G-sponges were grown by an in situ solvothermal process of graphene oxide (GO) sheets in ethanol.<sup>[17]</sup> These sponges

have an average transversal size of 1.5 cm and a thickness of about 1 cm (see **Figure 1b**). According to previous works,<sup>[17,18]</sup> the 2D graphene electronic behavior due to a Dirac-like band structure (see **Figure 1c**), is essentially preserved for the individual graphene sheets forming the G-sponge, while a weak band gap opens in proximity of the sheet interconnection regions.<sup>[17,18]</sup> The G-sponge samples here investigated show a flat reflectivity from IR to UV of about 5%, and a density of 0.92 kg m<sup>-3</sup>.

We investigated the sound emission as a function of excitation light wavelength covering the range from IR to UV by means of different nearly-monochromatic LEDs emitting at 1720, 1050, 780, 280 nm, respectively, and through a broadband white LED emitting in the visible range from 400 to 750 nm. LED emission spectra are reported in the Supporting Information.

We first discuss the results of acoustic generation in G-sponge by a sinusoidal modulated optical waveform. **Figure 1d** shows the emitted sound driven by a sinusoidally modulated white LED at different modulation frequencies having a rms optical power of 20 mW. The excitation optical waveform is instead reported in **Figure 1a** at 1 kHz. As one can observe, the acoustic wave is emitted at the modulating frequency of the optical excitation and its pressure amplitude increases with increasing frequency. This behavior is better shown in **Figure 1e**, where the emitted sound pressure level (in dB), is reported by red dots as a function of the modulation frequency for an optical power of 20 mW. SPL monotonically increases versus the modulation frequency showing, for frequencies above 10 kHz, a saturation behavior.

**Figure 1f–g** shows the acoustic pressure versus the optical power  $q_0$  at two different modulation frequency: 1 and 10 kHz. As one can clearly see from those panels, the acoustic pressure linearly depends on the input power and it is practically independent of the excitation wavelengths. This is also true for a broadband white LED. All these data indicate the same sound generation efficiency for wavelengths from 1720 nm (IR) to 280 nm (UV).

The wavelength independent acoustic behavior previously observed is determined by two different factors: (i) The photoacoustic effect investigated in this paper is related to intercone transitions in the Dirac band structure of graphene, sketched in **Figure 1c**. This results in a photon wavelength independent absorption coefficient<sup>[13]</sup>; (ii) At these photon wavelengths the dominant electronic cooling channel is the nonradiative electron–phonon scattering.<sup>[18]</sup> This implies, approximately, that the whole optical energy is converted into phonon population.

For higher photon energies, however, other nonradiative mechanisms take place, such as the emission of electrons by Auger-like effect<sup>[18]</sup> that can affect the efficiency of photo-thermal conversion.

The increase of lattice temperature due to the electron relaxation towards phonons leads to a thermal wave inside the G-sponge. Due to the low heat capacity of graphene this thermal energy is rapidly dissipated toward the air layers adjacent to the graphene interfaces. This generates a quick expansion of the air layers which act as an acoustic piston on the rest of surrounding gas column producing a pressure wave, i.e., a sound wave.

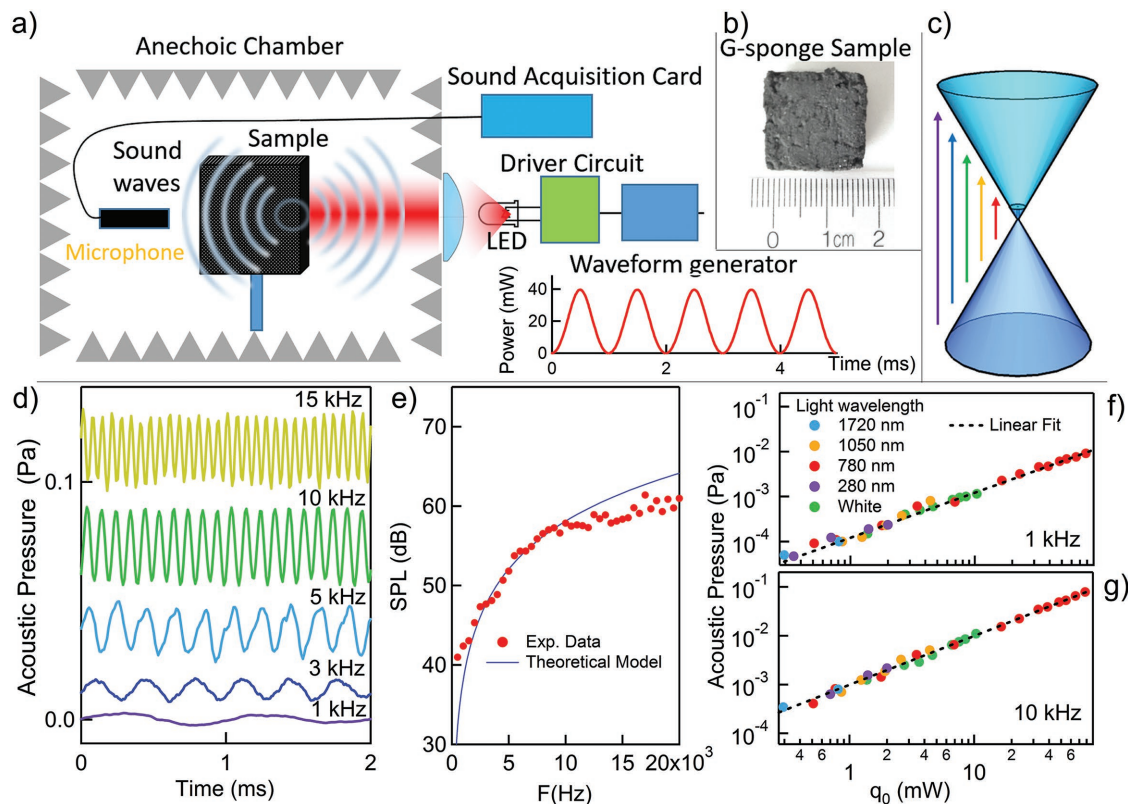


**Figure 1.** Sound generation from graphene sponge: a) scheme of experimental setup for acoustic generation measurements: intensity modulated light at different wavelengths and modulation frequencies is emitted by a LED powered by a driver circuit coupled with a waveform generator. The light then enters through a lens inside the anechoic chamber irradiating the G-sponge. b) View of the G-sponge sound emitter. c) Linear (Dirac) electronic band dispersion in graphene: The arrows represent the interband transitions under an optical excitation. The electrons involved relax by electron–phonon interaction inducing a lattice heating on fast (ps) time-scale. The fast-rise thermal gradient in the G-sponge network generates acoustic waves. d) Acoustic emission in time domain at different frequencies of a sinusoidally modulated white light with a rms power of 20 mW (vertical offset added). e) The generated sound pressure level as a function frequency with at 20 mW input power of sinusoidal light. Red dots represent the experimental data and the blue solid line corresponds to a model of thermoacoustic emission, which is described in the main text. f,g) Generated acoustic pressure versus rms optical power at 1 and 10 kHz, respectively. Dots with different colors indicate different wavelengths of excitation light: 1710, 1050, 780, 280 nm, and white light. Dashed line is a linear fit. The clear linear dependence of the acoustic pressure versus the optical power is independent of the light wavelength across the visible range.

As a result, light driven acoustic emission mechanism in G-sponge can be described in terms of a combination of two distinct processes characterized by different timescales: A photo-thermal and a thermoacoustic process. The energy relaxation in the photothermal mechanism is driven mainly by the electron–phonon scattering and occurs on a fast time scale of tens of picoseconds.<sup>[23–25]</sup> Through this effect, light energy absorbed by electronic intercone transitions, is mainly transduced in an out-of-equilibrium phonon populations. The thermal energy here accumulated is then transferred over a microsecond scale to the surrounding air (see the Supporting Information for the thermal properties of the G-sponge under illumination). The acoustic generation can be described through a model proposed by Hu et al.,<sup>[26]</sup> which calculates the thermoacoustic emission from a solid.

The effective thermal length  $\lambda_G = \sqrt{\alpha_G/(\pi F)}$ , where  $\alpha_G = 2.25 \times 10^{-6} \text{ m}^2\text{s}^{-1}$  is the graphene-sponge thermal diffusivity<sup>[27]</sup> and  $F$  is the acoustic frequency, represents the maximum spatial extension of the thermal waves in the G-sponge. For the G-sponge investigated in this paper and for acoustic frequency

higher than a few of Hz,  $\lambda_G$  is less than the sample thickness. In this limit, the sound pressure (rms value), according with the model of Hu et al., can then be expressed as<sup>[26]</sup>

$$p = \frac{R_0}{r_0} \frac{\gamma - 1}{\nu_g} \frac{e_g}{M e_g + e_G} (1 - R) I_0 \quad (1)$$

where  $e_g$  and  $\gamma$  are the thermal effusivity (i.e., the rate at which a specific material can exchange heat with the surrounding environment), and the heat capacity ratio of the surrounding gas, respectively.  $M$  is a frequency dependent factor which approaches 1 at high frequency.  $\nu_g$  is the sound velocity in the gas, and  $e_G = \sqrt{\kappa \rho_G C_G}$  is the thermal effusivity of the G-sponge. Here,  $\kappa = \alpha_G \rho_G C_G$  is the sponge thermal conductivity,  $\rho_G$  its mass density and  $C_G = 690 \text{ J kg}^{-1} \text{ K}^{-1}$  its heat capacity whose value has been measured in ref. [27]  $R \approx 0.05$ , is the G-sponge reflectivity, taking into account reflection loss.  $I_0 = q_0/A$  is the input light intensity, where  $q_0$  is the optical input power and  $A$  is the illuminated sponge surface.

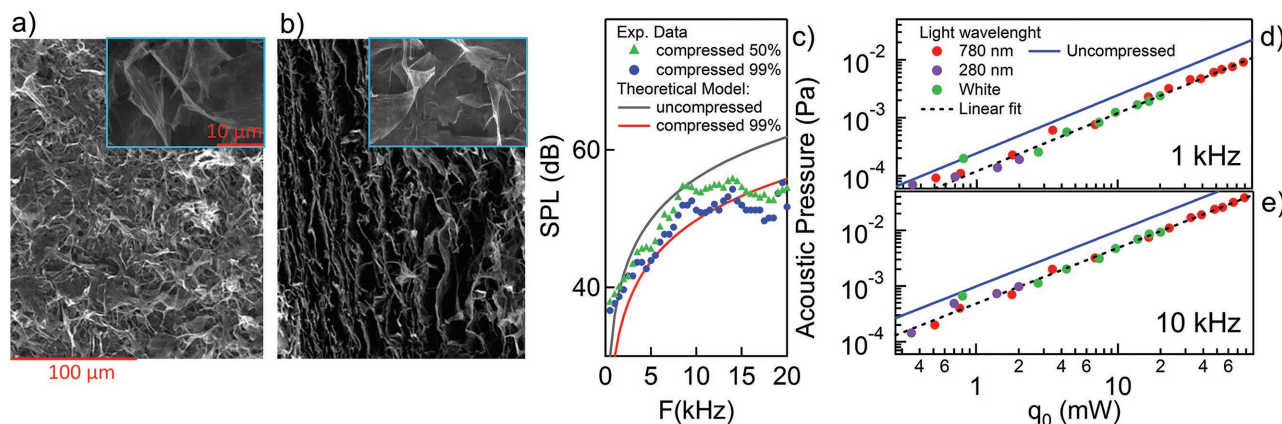


**Figure 2.** Effect of compressive strain on the sound generation efficiency in G-sponge. SEM images: a) G-sponge surface; b) G-sponge surface parallel to the compressive direction for a strain over 99% (plastic regime). Insets in a) and b) show magnified SEM images for G-sponge and 99% compressed G-sponge, respectively. At short-range the network morphology and the physical parameters of graphene sheets remain approximately unchanged. c) Generated SPL from compressed G-sponge 99% by a sinusoidal optical waveform with 20 mW rms power: Blue dots are experimental data, red solid line results from the thermoacoustic model for compressed G-sponge (see main text), while gray solid line corresponds to the thermoacoustic emission for the uncompressed G-sponge. Green triangles represent instead a 99% compressed G-sponge. Its sound emission intensity is intermediate between uncompressed and 99% compressed sample. d, e) Generated acoustic pressure versus the optical power for the compressed G-sponge at 1 and 10 kHz, respectively. Dots with different colors indicate different wavelengths of excitation light: 780 nm, 280 nm, white line. Dashed line is a linear fit. As a result, the conversion efficiency decreases with respect to uncompressed G-sponge (blue line). The 50% compressed G-sponge (not shown) has an intermediate efficiency.

In Equation (1),  $R_0/r_0$ , where  $R_0 = FA/v_g$  is the Rayleigh distance, and  $r_0$  is the distance between the sound source and the microphone, provides the right far-field limit where the experiments have been performed.

As shown in Figure 1e by a blue dashed line, Equation (1) quantitatively reproduces the sound pressure as a function of frequency without the use of free parameters. The disagreement between theory and experimental data at high frequency is under evaluation. The small size of the anechoic chamber used in the experiment is probably one of the origin of this behavior.

Moreover, the calculated acoustic pressure has a linearly dependence on the optical power  $q_0$  as experimentally observed. The slope calculated by Equation (1) is 0.07 (0.75) Pa  $W^{-1}$  at 1 kHz (10 kHz) which is very close to 0.08 (0.81) Pa  $W^{-1}$  experimentally obtained (see Figure 1f,g). The small difference between data and calculation are related to the uncertainties in the G-sponge thermal parameters entering in Equation (1).

## 2.2. Acoustic Waves Emission from Compressed G-Sponge

A crucial parameter of the photo thermoacoustic effect is the thermal effusivity  $e$ . Indeed, as observed in Equation (1), in order to obtain an efficient photo-thermoacoustic effect the effusivity of a material must be comparable to that of the surrounding gas. The effusivity in conventional bulk conductors is very high thus they are not suitable for thermoacoustic applications. This limitation has been partially overcome by fabricating thin and nanostructured materials in which the mass density and the heat capacity per unit area (HCPUA) are strongly reduced.<sup>[11,12,28,29]</sup>

In order to investigate the dependence of the acoustic emission on the G-sponge morphology, we have applied a compressive strain to the G-sponge sample increasing

the density from the initial value of 0.92 kg  $m^{-3}$  to nearly 2 kg  $m^{-3}$  (50% compression) and, finally, at about 10 kg  $m^{-3}$  (99% compression). SEM data of the uncompressed and highly compressed G-sponge (99% of applied strain), are represented in Figure 2a,b respectively. The as-grown sponge consists of a frame of interconnected microscale voids, resulting in an open-cell structure (Figure 2a). With an applied compressive strain of 99%, the G-sponge enters in a plastic deformation regime, where the void space shrinks and the sample becomes denser as shown in Figure 2b. Notably, the graphene-microvoid walls originally randomly distributed, stack in nearly parallel-aligned arrays perpendicular to the compressive strain direction. The 50% compressed sponge (not shown) presents a microscopic structure denser but morphological similar to the uncompressed one.

Figure 2c shows the sound pressure level versus frequency, generated from the two compressed G-sponges (green triangles 50% compression, blue points 99% compression, respectively), in comparison to the uncompressed sample (black line). All sponges are illuminated by a sinusoidally modulated white LED at 20 mW rms power. The overall behavior of SPL for the compressed sponges is similar to that of uncompressed sample, e.g., it increases with frequency. While, the G-sponge with a density of 2 kg  $m^{-3}$  (50% compression, green triangles) shows an intermediate sound level with respect to the uncompressed one, the mostly compressed sample (10 kg  $m^{-3}$ , 99% compression), presents the lowest sound pressure (about a factor 2 of reduction, blue points). This means a reduction in the photoacoustic conversion efficiency of about a factor 4. A reduced efficiency is also observed in Figure 2d,e which show the acoustic pressure for the mostly compressed sample versus the input optical power at two different frequencies (1 and 10 kHz), compared with the uncompressed results (colored points and continuous blue line, respectively).

At a very high compressive strain, anisotropy is induced into the sponge, and a growing alignment of the graphene sheets perpendicular to the direction of compression occurs (see Figure 2b). This leads to a final plastic deformation of the sample determining a long-range (millimeter) order, keeping intact, instead, the short spatial structure (micrometer) of the graphene sponge network, as confirmed by SEM image in the insets in Figure 2a,b. In particular, the macroscopic order does not affect the thermal and optical properties of the individual sheets. Therefore, the reduction of the sound emission efficiency is mainly due to the increase of the G-sponge density which reduces the sponge effusivity  $e_G$ . This behavior is further confirmed by putting the density of the mostly compressed G-sponge in Equation (1). The numerical results, shown through a red curve in Figure 2c, well reproduce the experimental data.

### 2.3. Coherent Acoustic Wave Emission

As previously described, a sound wave is generated when graphene-sponge samples are shined by a modulated light. The sound power is linearly dependent on the light intensity and independent of the light wavelength from infrared to ultraviolet.

In order to investigate the time scale formation of the sound wave, in this subsection we study the acoustic generation as a function of the rise time of a square-wave optical-excitation. The square wave from a white LED at different rise times are reported in Figure 3a by red lines, while the corresponding sound waves are shown by colored lines. A narrow acoustic

pulse appears when the optical rise time is less than a few tens of  $\mu\text{s}$ . For these time-scales a broadband pulse is generated in the frequency domain, as shown in Figure 3b from 20 Hz to 16 kHz. An increase of the rise time determines a temporal broadening of the acoustic pulses, which reflects in a reduction of their intensity and spectral distribution in the frequency domain.

The acoustic wave emitted, in the same optical conditions, for a rise time less than  $1\ \mu\text{s}$  and a repetition rate frequency of 100 Hz, is shown in Figure 3c as a function of time. Each period has two optical edges, corresponding to the rising and falling of the light wavefront, which are labeled in Figure 3c, by a sign (+) and (-), respectively. An expansion pressure wave is then generated in correspondence of the optical rise time. This is due to a fast heating of the graphene sponge above room temperature (the thermal properties of graphene sponge under illumination have been reported in Video S1 of the Supporting Information). At the optical falling time, a fast cooling process toward room temperature is instead produced inducing a compression pressure wave (Figure 3c). The expansion and compression waves actually present an exact specular shape.

Increasing the repetition rate of the optical square wave for a fixed optical power, the time dependence of the acoustic waveform changes significantly (see Figure 3d). This effect can be ascribed to a progressive temporal superposition of the expansion and compression waves. In particular, the heating-cooling waves are constructively overlapped when the frequency approaches 10 kHz resulting in an effective increase of the acoustic pressure. For higher frequencies instead, heating-cooling waves begin to destructively interact decreasing the

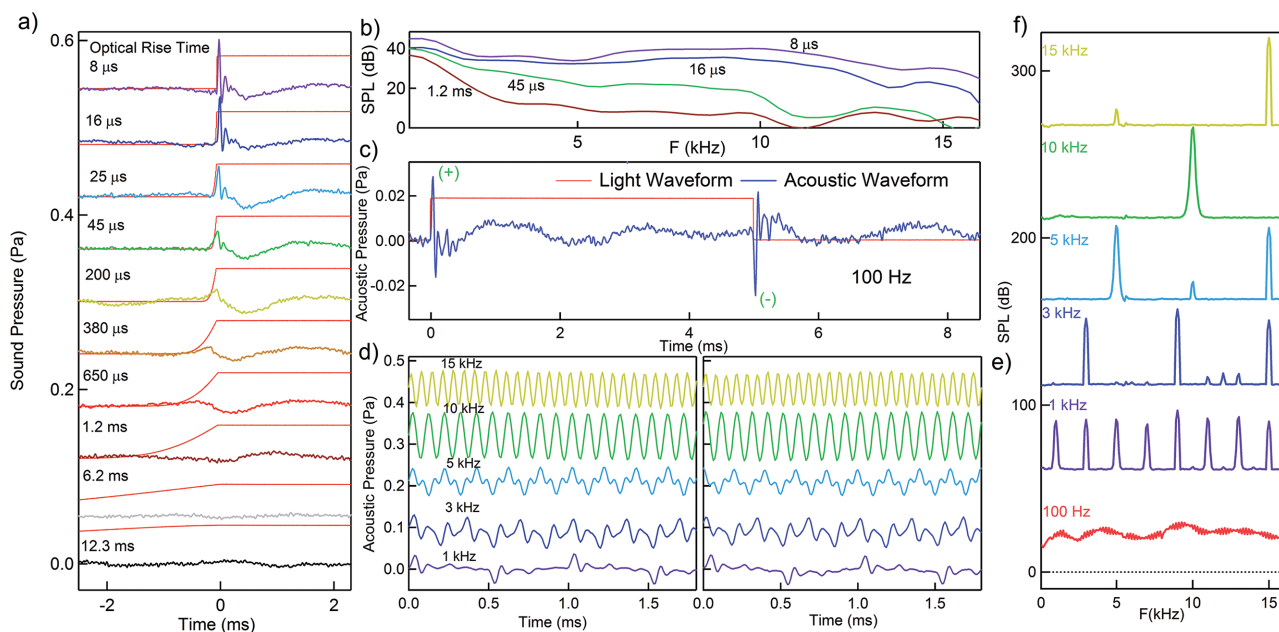


**Figure 3.** Broadband acoustic generation from optical square-wave in G-sponge: time and frequency domain. a) Temporal profile of the acoustic pulse generate in G-sponge as a function of rise time of an optical square-wave which is shown by a red curve (vertical offset added). b) Related acoustic spectra for different rise time. c) Generated acoustic wave (blue curve) by an optical square-wave (red curve) with 100 Hz modulating frequency. d) Time domain signal of G-sponge sound at different modulation frequencies of the optical square wave. A vertical offset has been applied to the curves for a clearer view. e) Numerical simulation of the temporal overlapped acoustic waves. f) Evolution of the emission spectrum versus the amodulation frequency. All measurements were performed with a white LED optical waveform with a power of 20 mW.

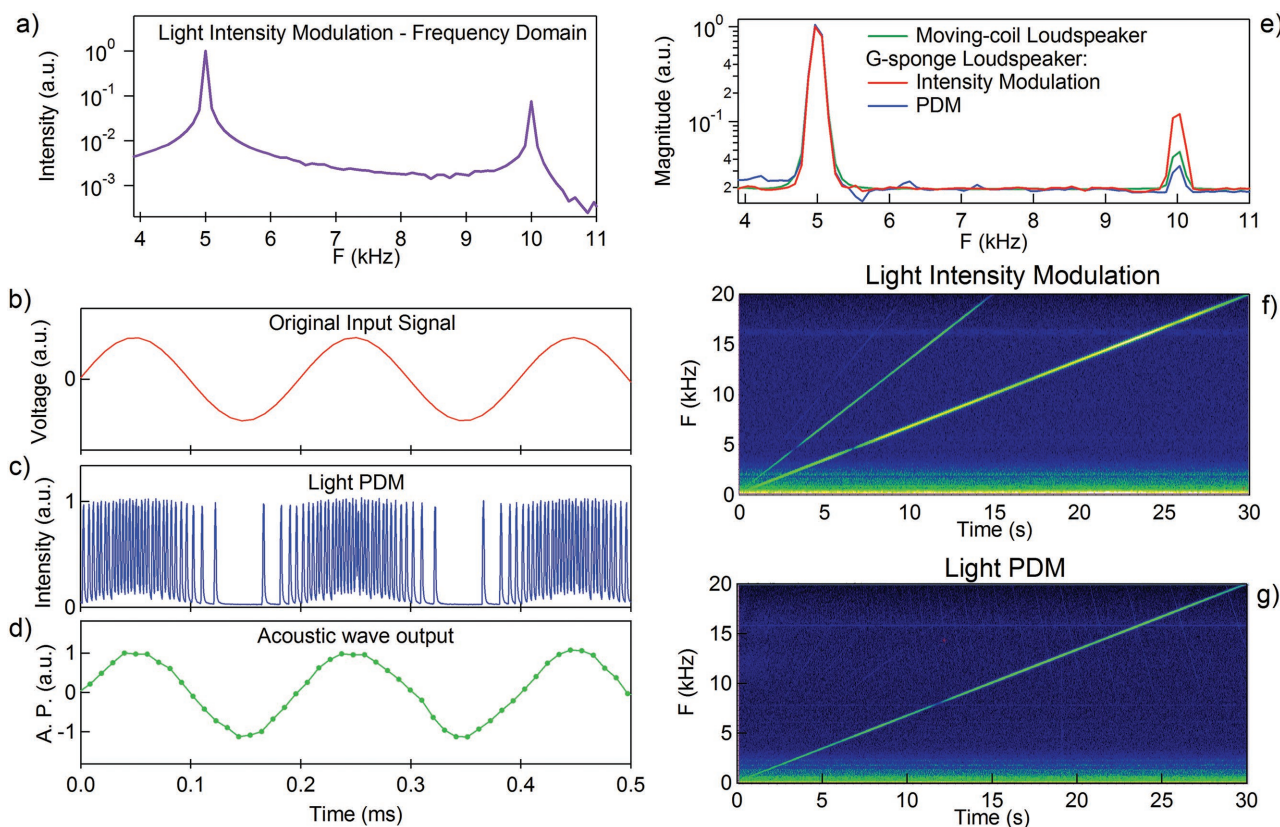


**Figure 4.** Light pulse density modulation: a) Sinusoidally intensity modulated light in frequency domain emitted from a white LED. Modulation frequency is 5 kHz. The LED response induces a distortion of emitted light waveform and consequently a first harmonic is observed at 10 kHz. b) Waveform of an analog input signal (5 kHz). c) The corresponding light pulse trains from PDM-digitized analog signal. d) Measured acoustic output signal. This full digital operation mode very well reproduces the analog input signal. e) Acoustic wave emitted in the G-sponge through the intensity modulation mode (red curve), PDM mode (blue curve). The corresponding acoustic wave emitted from a commercial moving-coil loudspeaker at 5 kHz (green curve). f) Time-frequency plot of generated acoustic waves of linear swept-frequency input signal by intensity modulation mode (see main manuscript). g) Corresponding generation acoustic waves by PDM mode. As one can observe the harmonic distortion is strongly suppressed.

emitted acoustic pressure as observed, for instance, at 15 kHz in Figure 3d.

In order to simulate this overlapping effect we performed a numerical calculation. In this simulation (see Figure 3e), the acoustic pulses at 100 Hz (see Figure 3c), which can be considered as noninteracting, have been superimposed with alternating signs. By increasing the modulation frequency up to 15 KHz, i.e., by reducing the period among two consecutive pulses, the simulation accurately reproduces both the shapes and the intensities of the measured acoustic waves. This superposition effect clearly influences the sound spectral distribution as observed in Figure 3f. From a broadband spectrum generated by a single acoustic pulse (at 100 Hz), the sound spectral distribution evolves in a comb spectrum of odd harmonics of the modulation frequency (from 1 to 15 kHz). This agrees to the fact that the Fourier expansion of a square wave contains only odd harmonics.

## 2.4. Light-Driven Loudspeaker

The first light-driven loudspeaker was proposed in 1983 by Rush et al. which, following the Bell's idea, generated sound

through an intensity modulated laser beam in a gas.<sup>[30]</sup> This device was able to overcome the mechanical limitations of the conventional loudspeaker achieving high fidelity sound reproduction. However, due to the very weak gas photoacoustic efficiency and therefore the need of a powerful laser system, the spread of this device was limited. The light-sound transducer based on G-sponges investigated in this manuscript has instead, due to its high efficiency and fidelity, a huge potentiality for new applications, in particular as loudspeaker and broadband light detector.

Despite the linearity of the photo-thermoacoustic effect in G-sponge, LED sources shows a weak nonlinear behavior which leads to a small distortion of the light output waveform. This represents a drawback in the generation of acoustic waves using the light intensity modulation scheme. As a result, one generates both the fundamental modulation frequency and high order harmonics which may distort consequently the acoustic output (see Figure 4a).

In order to generate a pure tone and achieving a high fidelity in sound reproduction, G-sponge loudspeaker can be driven by a light pulse density modulation (PDM) method.<sup>[31]</sup> In PDM mode, an analog input signal is encoded in sequential pulse trains with constant height and a relative temporal pulse

density that corresponds to the analog signal's amplitude. A sinusoidal analog waveform (5 kHz), is encoded by PDM in a digital signal which drives the LED (Figure 4b). The generated light pulse trains measured by a photodiode, where a single light pulse has an Full Width Half Maximum (FWHM) of 1  $\mu$ s, are shown in Figure 4c. The acoustic output signal is instead shown in Figure 4d. We can see that from a light pulse density modulated signal the original analog signal is well reproduced.

The generated acoustic wave in frequency domain is reported in Figure 4e. The first harmonic intensity, which, in the intensity modulation scheme, is nearly 10% of the fundamental one, decreases to about 1% in the PDM mode. The distortions in the light driven loudspeaker based on G-sponge are lower than the typical value of the commercial moving-coil loudspeaker (HP S5000 2.0), as shown in Figure 4e. Even better results can be obtained by reducing the duration of the single light pulse and increasing the digital sampling of the analog input waveform.

Figure 4f,g shows the time-frequency plots for linear swept-frequency sine input signal from 200 Hz to 20 kHz by using light intensity modulation and PDM mode, respectively. Let us further observe that the high order harmonics introduced by the nonlinear response of the LED are strongly suppressed using the PDM method.

Therefore, G-sponge loudspeaker is compatible with the PDM sampling technique, permitting a full digital operation integrable with other electronic devices and providing an ultrahigh sound fidelity with frequencies from acoustic to ultrasound. The capability of a G-sponge light speaker in reproducing a real audio file is shown in Video S2 of the Supporting Information. Here, G-sponge based-speaker is able to play songs by intensity modulated light with a 20 mW power generated from a commercial with LED.

## 2.5. Conclusions and Perspectives

In this work, we have presented an unprecedented concept of photoacoustic speaker taking advantage of the outstanding thermodynamic, mechanical and optical properties of a free-standing 3D graphene sponge structure. This material, which have a density similar to air, provides an unparalleled lightness and mechanical stability of the loudspeaker while the absence of the substrate, preventing the thermal leakage, enhances the photoacoustic energy conversion and the efficiency of the device. The light-driven acoustic generation allows to emit sound from far distances without any type of physical connection. Moreover, the heat distribution on the sponges can be fully controlled by the spatial distribution of the light giving rise to a stereoscopic device with an acoustic power linearly dependent on the illuminated surface and independent of the light wavelength from infrared to ultraviolet. The present results suggest that the light-driven acoustic generation in graphene sponge could be widely used in a variety of new technological applications from sound and ultrasound production, radiation detectors and medical devices.

## Supporting Information

Supporting Information is available from the Wiley Online Library or from the author.

## Acknowledgements

T.Z., K.Z., Y.C. fabricated and characterized 3D graphene sponges. F.G., S.L., A.M., M.S., L.D.T., C.V. carried out the infrared, visible, and ultraviolet experiments. Data analysis was performed by F.G. and L.D.T. F.G. and S.L. planned and managed the project with inputs from all the co-authors. F.G. and S.L. wrote the manuscript. All authors extensively discussed the results. With the contribution of the Italian Ministry of Foreign Affairs and International Cooperation, Directorate-General for the promotion of the country system.

## Conflict of Interest

The authors declare no conflict of interest.

## Keywords

acoustic devices, graphene, photoacoustic emission, photoacoustic speakers, ultrasound emission

Received: May 17, 2017  
Revised: September 6, 2017  
Published online:

- [1] C. Sachs, *History of Musical Instruments*, Dover Publications, Mineola, New York **2006**.
- [2] J. Borwick, *Loudspeaker and Headphone Handbook*, CRC Press, Boca Raton, Florida **2012**.
- [3] A. Bell, *J. Soc. Electr. Eng.* **1880**, 9, 305.
- [4] J. Tyndall, *Proc. R. Soc. London* **1880**, 31, 307.
- [5] W. Röntgen, *Philos. Mag. Ser. 5* **1881**, 11, 308.
- [6] A. Bell, *Philos. Mag. Ser. 5* **1881**, 11, 510.
- [7] D. W. Ball, *Chem. Fac. Publ.* **2006**, 131, 21.
- [8] H. Arnold, I. Crandall, *Phys. Rev.* **1917**, 10, 22.
- [9] L. Xiao, Z. Chen, C. Feng, L. Liu, Z. Bai, Y. Wang, L. Qian, Y. Zhang, Q. Li, K. Jiang, S. Fan, *Nano Lett.* **2008**, 8, 4539.
- [10] Y. Wei, X. Lin, K. Jiang, P. Liu, Q. Li, S. Fan, *Nano Lett.* **2013**, 13, 4795.
- [11] R. Dutta, B. Albee, W. van der Veer, T. Harville, K. Donovan, D. Papamoschou, R. Penner, *J. Phys. Chem. C* **2014**, 118, 29101.
- [12] H. Tian, D. Xie, Y. Yang, T. Ren, Y. Wang, C. Zhou, P. Peng, L. Wang, L. Liu, *Appl. Phys. Lett.* **2011**, 99, 043503.
- [13] K. Mak, L. Ju, F. Wang, T. Heinz, *Solid State Commun.* **2012**, 152, 1341.
- [14] H. Tian, T. Ren, D. Xie, Y. Wang, C. Zhou, T. Feng, D. Fu, Y. Yang, P. Peng, L. Wang, L. Liu, *ACS Nano* **2011**, 5, 4878.
- [15] J. Suk, K. Kirk, Y. Hao, N. Hall, R. Ruoff, *Adv. Mater.* **2012**, 24, 6342.
- [16] H. Tian, D. Xie, Y. Yang, T. Ren, Y. Wang, C. Zhou, P. Peng, L. Wang, L. Liu, *Nanoscale* **2012**, 4, 2272.
- [17] Y. Wu, N. Yi, L. Huang, T. Zhang, S. Fang, H. Chang, N. Li, J. Oh, J. Lee, M. Kozlov, A. Chipara, H. Terrones, P. Xiao, G. Long, Y. Huang, F. Zhang, L. Zhang, X. Lepró, C. Haines, M. Lima, N. Lopez, L. Rajukumar, A. Elias, S. Feng, S. Kim, N. Narayanan, P. Ajayan, M. Terrones, A. Aliev, P. Chu, Z. Zhang, R. Baughman, Y. Chen, *Nat. Commun.* **2015**, 6, 6141.
- [18] T. Zhang, H. Chang, Y. Wu, P. Xiao, N. Yi, Y. Lu, Y. Ma, Y. Huang, K. Zhao, X. Yan, Z. Liu, J. Tian, Y. Chen, *Nat. Photonics* **2015**, 9, 471.
- [19] L. Jiang, Z. Fan, *Nanoscale* **2014**, 6, 1922.
- [20] H. Hu, Z. Zhao, W. Wan, Y. Gogotsi, J. Qiu, *Adv. Mater.* **2013**, 25, 2919.
- [21] W. Wan, L. Li, Z. Zhao, H. Hu, X. Hao, D. Winkler, L. Xi, T. Hughes, J. Qiu, *Adv. Funct. Mater.* **2014**, 24, 4915.

- [22] C. Zhao, C. Yu, S. Liu, J. Yang, X. Fan, H. Huang, J. Qiu, *Adv. Funct. Mater.* **2015**, 25, 6913.
- [23] H. Wang, J. Strait, P. George, S. Shivaraman, V. Shields, M. Chandrashekar, J. Hwang, F. Rana, M. Spencer, C. Ruiz-Vargas, J. Park, *Appl. Phys. Lett.* **2010**, 96, 081917.
- [24] I. Gierz, J. Petersen, M. Mitrano, C. Cacho, I. Turcu, E. Springate, A. Stöhr, A. Köhler, U. Starke, A. Cavalleri, *Nat. Mater.* **2013**, 12, 1119.
- [25] Y. Tian, H. Tian, Y. Wu, L. Zhu, L. Tao, W. Zhang, Y. Shu, D. Xie, Y. Yang, Z. Wei, X. Lu, T. Ren, C. Shih, J. Zhao, *Sci. Rep.* **2015**, 5, 10582.
- [26] H. Hu, T. Zhu, J. Xu, *Appl. Phys. Lett.* **2010**, 96, 214101.
- [27] A. Aliev, N. Mayo, M. Jung de Andrade, R. Robles, S. Fang, R. Baughman, M. Zhang, Y. Chen, J. Lee, S. Kim, *ACS Nano* **2015**, 9, 4743.
- [28] A. Niskanen, J. Hassel, M. Tikander, P. Maijala, L. Grönberg, P. Helistö, *Appl. Phys. Lett.* **2009**, 95, 163102.
- [29] H. Tian, D. Xie, Y. Yang, T. Ren, Y. Lin, Y. Chen, Y. Wang, C. Zhou, P. Peng, L. Wang, L. Liu, *Appl. Phys. Lett.* **2011**, 99, 253507.
- [30] W. Rush, J. Huebler, P. Lysenko, *J. Acoust. Soc. Am.* **1989**, 85, 529.
- [31] N. Koshida, D. Hippo, M. Mori, H. Yanazawa, H. Shinoda, T. Shimada, *Appl. Phys. Lett.* **2013**, 102, 123504.